

## An Inverse Model for Predicting Reservoir Structure and Thermal Lifetime using Inert and Adsorbing Tracers

Adam J. Hawkins<sup>1,2</sup>, Don Fox<sup>2,3</sup>, Matthew Becker<sup>4</sup>, and Jefferson Tester<sup>1,2,3</sup>

<sup>1</sup>Cornell University, Earth and Atmospheric Sciences, Ithaca, NY 14853

<sup>2</sup>Cornell University, Cornell Energy Institute, Ithaca, NY 14853

<sup>3</sup>Cornell University, Smith School of Chemical and Biomolecular Engineering, Ithaca, NY 14853

<sup>4</sup>California State University, Long Beach, Geology Department, Long Beach, CA 90840

ajh338@cornell.edu

**Keywords:** inert; reactive; tracers; inversion; thermal performance; field test; adsorption; fracture aperture; genetic algorithm; principal component analysis

### ABSTRACT

The focus of this research is the development and field testing of an inverse model for predicting the thermal hydraulic performance of fracture-dominated geothermal reservoirs with spatially-varying permeability. The inverse model utilizes Principal Component Analysis (PCA) and a Genetic Algorithm (GA) to identify a representative permeability distribution. Field testing was conducted at a meso-scale field site, referred to as the “Altona field site,” which serves as a geothermal analog. The inverse model identifies a two-dimensional, spatially correlated permeability field by minimizing an objective function relating measured and simulated inert and adsorbing tracer RTDs. The resulting permeability distribution was subsequently used to forecast the spatial distribution of heat transport and predict thermal breakthrough at the production well. A two-spot pattern was utilized with an injection to production well separation of 14 m. The wells are connected by a sub-horizontal fracture at 7.6 m below ground surface. Preliminary results suggest that the inverse model successfully predicts early thermal breakthrough resulting from the continuous circulation of hot water (74 °C) through the relatively cold formation, initially at 11 °C. The identified permeability field suggests that a narrow flow channel (~1-2 m) was responsible for the occurrence of rapid thermal breakthrough. The results are corroborated by Ground Penetrating Radar (GPR) imaging of the target fracture and tracer transport as well as measurements of the spatial distribution of fracture/matrix heat exchange.

### 1. MOTIVATION AND SCOPE

In geothermal reservoirs that actively inject cold water, reservoir modeling is commonly used to forecast thermal drawdown at production wells. To accomplish this goal, one must have sufficient insight into the spatial distribution of fluid flow paths between injection and production wells. In sparsely-spaced fracture-dominated reservoirs, it is the fracture surface area available for heat exchange between circulating fluids and the bulk rock matrix, or “flow-wetted area” (FWA), which is critically important in forecasting thermal performance (Hawkins et al., 2017a). Ideally, there is sufficient FWA such that the cold injection fluid is adequately heated by the hot reservoir rock before reaching the production well. If FWA is insufficient, however, production well fluid temperature will decline below plant design specifications prior to the end of the project’s planned lifetime. In this case, the production well has experienced “premature thermal breakthrough” leading to poor thermal performance, which could be disastrous for a commercial geothermal reservoir.

Tracer testing is a common reservoir characterization technique for investigating subsurface fluid flow in many industries, including geothermal (Shook, 2003). After injecting one or more inert solutes, a conventional tracer test involves monitoring tracer concentration through time at producers. A plot of the tracer concentration versus time provides a Residence Time Distribution (RTD) which is an invaluable dataset for evaluating flow connectivity between injectors and producers.

In addition, tracer RTDs are commonly used for calibrating fluid flow models which are subsequently used to forecast thermal performance (e.g., Axelsson et al., 2001; Axelsson et al., 2005; Kristjánsson et al., 2016; Robinson et al., 1988; Shook, 2001; etc.). In many applications, a tracer RTD is fit using an analytical solution for tracer transport which includes the influence of advection and dispersion in a single flow channel or in a two-dimensional fracture with uniform aperture. Fitted parameters typically include the fracture aperture and the Peclet Number. The Peclet Number is the ratio of advection and hydrodynamic dispersion within the plane of a fracture; high Peclet Numbers indicate advection dominates.

The classical approach for defining hydrodynamic dispersion in a porous medium is based on the assumption that the process is Fickian (e.g., Taylor-Aris Dispersion) (National Research Council, 1996, p.273). The validity of this assumption is questionable, however, particularly in rough fractures with spatially varying apertures that produces flow “channeling” (e.g., Bodin et al., 2003; Dagan, 1986; Gelhar, 1986; Neretnieks, 1983; Tsang and Neretnieks, 1998). In these cases, the spread of the tracer RTD may be influenced by Taylor-Aris dispersion, roughness dispersion, and by flow channeling. In such a reservoir, a hydrodynamic dispersion coefficient derived from an inert tracer test RTD will appear to be larger than expected based on dispersion described by Taylor-Aris. Additional factors that can

obscure the nature of dispersion in tracer RTDs include wellbore dilution, adsorption, matrix diffusion, and time scale dependencies (e.g., Reimus et al., 2003; Bodin et al. 2003; Moench, 1989, 1995).

The ambiguity of dispersion mechanisms substantially hinders the reliability of thermal forecasts based on calibrations using inert tracer RTDs. Substantial inaccuracies can be introduced in thermal forecasting because it is unclear how to incorporate dispersion derived from a tracer test in heat transport simulations. According to Taylor-Aris dispersion, heat transport should experience negligible dispersion within the fracture because the high diffusivity of heat negates the influence of velocity profiles within a fracture. This would suggest that dispersion derived from a tracer test can be neglected in heat transport simulations. However, if the dispersion observed in a tracer RTD resulted from flow channeling, this assumption would be inappropriate, because flow channeling can have a substantial influence on FWA and thus strongly influence thermal performance.

Because of uncertain dispersion mechanisms and the possibility of flow channeling, there is a need for the following advancements: (1) a tracer that interrogates FWA; and (2) an inverse model that identifies spatially varying permeability fields. This article is the latest in a series that discuss heat and tracer experiments at the Altona field site (Hawkins et al., 2017a, 2017b). It presents a novel inverse model for identifying spatially varying permeability fields using inert and adsorbing tracers. The model is tested using the results of a series of field experiments in which inert and adsorbing tracer tests were conducted in addition to a heat exchange experiment in which thermal breakthrough was measured.

## 2. BACKGROUND

### 2.1 Field Site

The field site is located in the Altona Flat Rocks, in northern New York State, USA about 6 km northwest of West Chazy. The Altona Flat Rocks region is unique in the Northeastern United States, because a glacial flood stripped soil overburden off large regions of bedrock, exposing an expanse of sandstone with shallow groundwater in bedrock fractures (Rayburn et al., 2005). The relevant formation, the Cambrian-aged Potsdam Sandstone, is well cemented with silica and as a consequence has a matrix (or “primary”) porosity of roughly 1 percent. Ubiquitous fracturing, however, makes the formation highly permeable and it is commonly used as an aquifer for drinking water (Olcott, 1995).

The well field is located near an abandoned dam (Skeleton Dam) which creates a hydraulic gradient of roughly 0.004 [-] across the well field as water flows from the artificial reservoir (Chasm Lake) to a small ledge which produces a seepage face (Becker and Tsoflias, 2010) (Figure 1). A five-spot 15 cm diameter well pattern penetrates a conductive sub-horizontal fracture 7.6 m below the surface. Transmissivity of the fracture is estimated to be about 5 m<sup>2</sup>/day which suggests a mean hydraulic aperture of roughly 0.5 mm based upon an analysis of slug tests performed at the Altona well field (Talley et al., 2005).

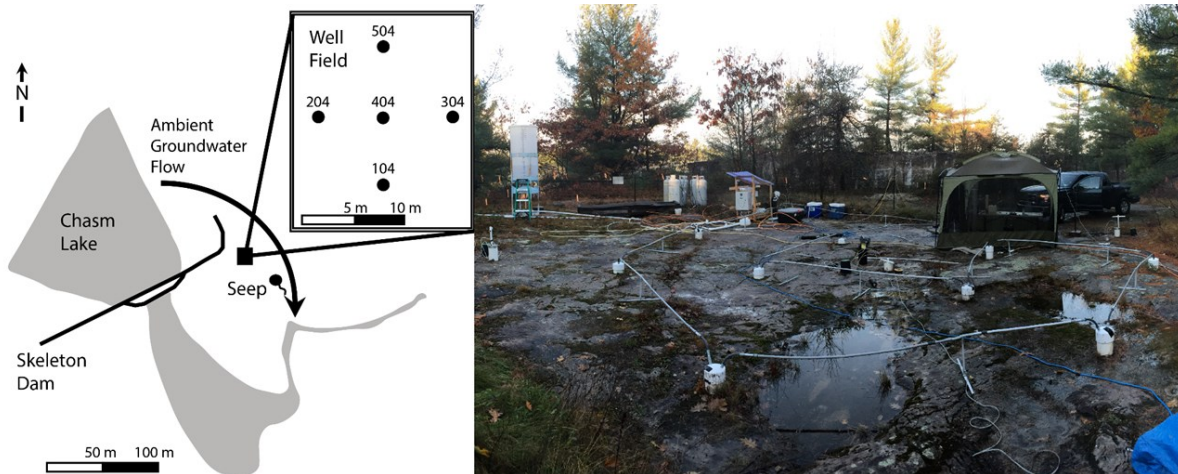


**Figure 1: Map of the Altona field site and well field (left) and a photograph of the well field taken in October 2015 (right).**

### 2.2 Associated Studies

#### 2.2.1 Ground Penetrating Radar (GPR)

In the summer of 2010, surface-based reflection GPR was used to image fracture fluids at the Altona field site. Two kinds of measurements were used; a “background” survey in which natural water is in place and a “saline” survey in which a saline solution is continuously circulated between an injection and production well. GPR imaging without saline solution provides a relative measure of the spatial distribution of fracture aperture, because a larger water-filled aperture leads to a greater reflection amplitude measured at ground surface (Tsoflias and Becker, 2008). GPR imaging with saline solution produces a combined measure of the spatial distribution of fracture aperture and saline tracer. Subtracting the background survey from the saline survey isolates the spatial distribution of saline tracer from the fracture aperture.

In these imaging experiments, saline water was injected in well 304 and pumped from well 204 (Tsoflias, 2013). The well pairs used in the tracer imaging experiments are the same as in this study, however, the flow direction is reverse. Amplitude measurements in pairs of 100 MHz antennae oriented orthogonal to one another were summed, to remove the effect of polarization from the reflected signal (Tsoflias et al., 2015).

The results of the GPR surveys conducted prior to this study indicate a spatially correlated and anisotropic distribution of fracture aperture. The spatial distribution of fracture aperture is represented by the strength of the amplitude, measured in relative amplitude units. Therefore, the areas of largest fracture aperture exist where the greatest amplitudes were measured. The results shown in Figure 2 reveal a narrow region of large aperture which persists in a direction oblique to the direct path between wells 204 and 304 at an angle of 25° to the south. The channel is roughly 1 to 2 m in width based on the extent of amplitude measurements in the range of -700 to -1200. The background survey therefore reveals potential for flow channeling between wells 204 and 304.

The GPR salt tracer imaging reveals a strong, direct flow path directly between the injection and production well over a distance of 14.1 m. The spatial distribution and concentration of saline tracer is represented by the strength of the amplitude difference, measured in relative amplitude units, between the amplitude measured prior to and during tracer circulation. Therefore, the areas of greatest tracer concentration existed where the greatest amplitude was measured. The width of the flow channel directly connecting the two wells is roughly 1 to 2 m in width based on the extent of the amplitude difference in the range of -100 to -500.

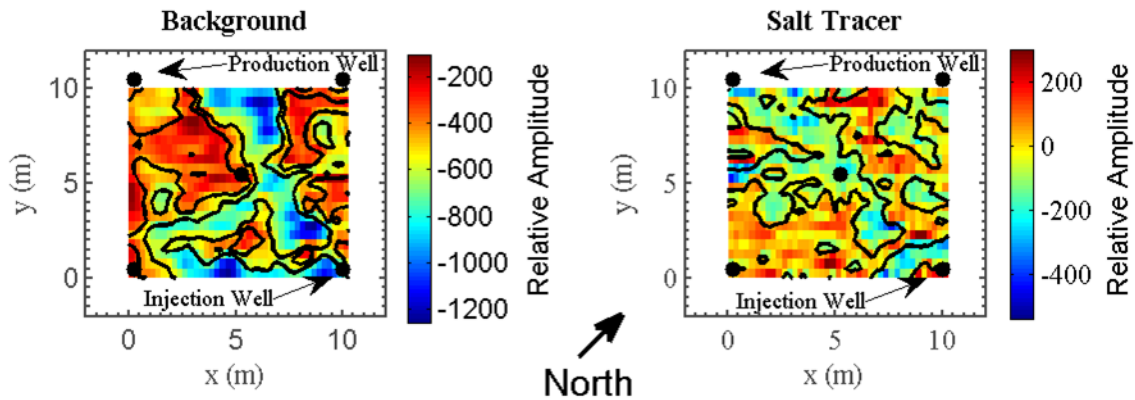


**Figure 2: Map of the background (left) and the saline (right) GPR survey. The background figure provides a relative measure of the fracture aperture distribution where a greater negative reflection amplitude (blue colors on the figure) represent larger fracture aperture. The saline GPR survey provides an estimate of wetted area where a more negative amplitude difference represents higher fluid salinity and, therefore, flow concentration. Note the flow was from well 304 to well 204 in the saline survey but from well 204 to well 304 in the heat exchange experiment and tracer tests that are the focus of this paper.**

### 2.2.2 Heat Transport

In the fall of 2015, the Altona field site was used as an analog meso-scale geothermal reservoir. During these experiments, hot water (74°C) was continuously injected into the relatively cold formation (11°C) for a period of 6 days. The injection and production well are separated by 14 m and a continuous flow rate of 5.7 L/min was maintained. While the reservoir was heated, temperature measurements were made in the production well, and within the rock matrix at various positions throughout the five-spot well field using Fiber-Optic Distributed Temperature Sensing (FODTS) (see Hawkins et al. (2017b) for details).

After 6 days of hot water circulation, the fracture fluid temperature increase observed in the 11 monitoring locations ranged from 0.9°C to 31.1 °C. The boreholes which experienced the greatest temperature rise were spatially distributed in a narrow path directly between the injection well and production well (Figure 3). At the production well, groundwater temperature ranged between 11.72 and 11.75 °C until the onset of thermal breakthrough 40 mins after the initiation of hot water injection (Figure 4). Thermal breakthrough roughly followed a logarithmic time dependence at late time. Reservoir fluid temperature at the production well rose 17.4 °C from 11.7 °C to 29.8 °C which corresponds to 29% of the difference between the initial temperature of groundwater pumped at well 304 and the temperature of water reinjected into well 204 (74 °C).

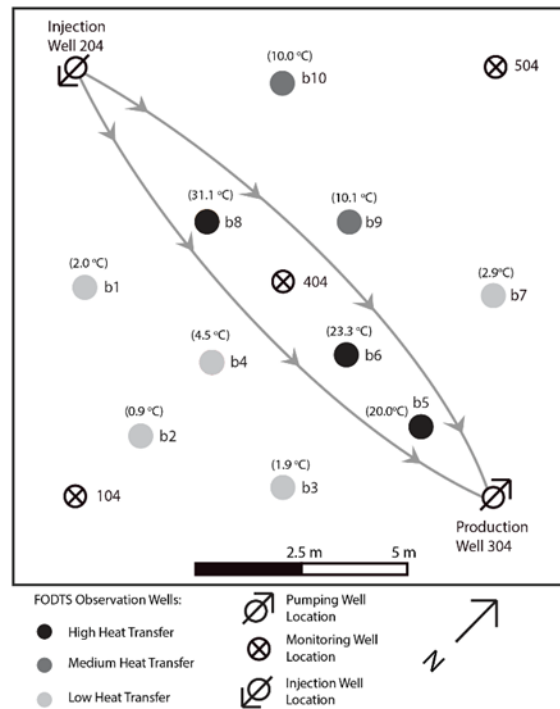


**Figure 3:** Map view representation of temperature rise, as recorded via FODTS after 144 hrs of hot water circulation. Values in parenthesis are the fracture fluid temperature rise. The grey arrows represent the general direction of fluid transport in the fracture from the injection well to the production well.

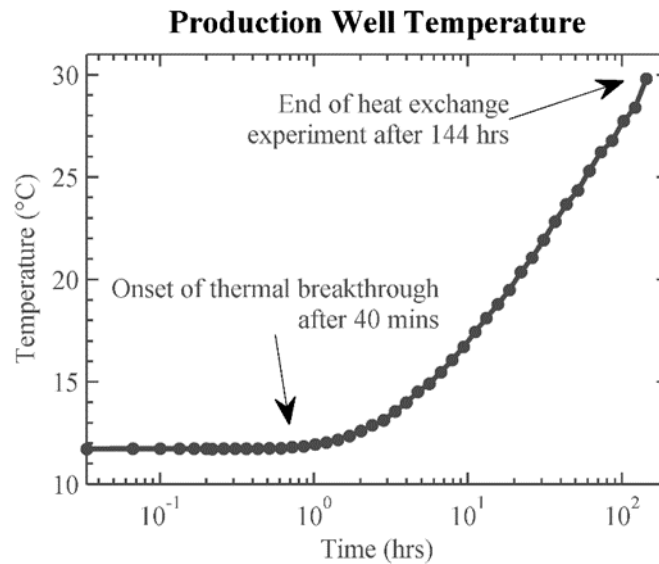


**Figure 4:** Measured production well temperature as a function of time on a log scale for the entire 144 hr experiment. The onset of thermal breakthrough at the production well occurred after 40 mins of hot water injection which corresponds to a temperature increase of 0.1% of the difference in injection and background temperature.

### 3. METHODS

#### 3.1 Adsorbing Tracers

An adsorbing tracer experiences mass transfer between the liquid phase and the solid rock phase. This transfer is controlled by the chemical properties of the solute and fracture surface as well as the solute concentration. For an adsorbing tracer, the advection-dispersion-reaction equation for tracer transport in a heterogeneous two-dimensional fracture is

$$w \frac{\partial c}{\partial t} = w \nabla \cdot (\mathbf{D}_f \cdot \nabla c) - w \langle \mathbf{v} \rangle \cdot \nabla c - \frac{\partial f}{\partial t}, \quad (1)$$

where  $w$  is the fracture aperture [L],  $c$  is concentration in the fracture [M/L<sup>3</sup>],  $t$  is time,  $f$  is tracer surface concentration [M/L<sup>2</sup>],  $\mathbf{D}_f$  is the two-dimensional dispersion coefficient tensor [L<sup>2</sup>/t], and  $\langle \mathbf{v} \rangle$  is the velocity vector [L/t]. The spatial dimension of the concentration gradient  $\nabla c$  is in the two-dimensional plane of the fracture.  $\mathbf{D}_f$  is a second-order tensor describing hydrodynamic dispersion in the two-dimensional fracture plane. It is a function of fluid velocity, longitudinal dispersivity,  $\alpha_L$  and chemical diffusion,  $D^*$ , and is expressed as (Bear, 1972)

$$\mathbf{D}_f = \alpha_L \frac{\langle \mathbf{v} \rangle \otimes \langle \mathbf{v} \rangle}{|\langle \mathbf{v} \rangle|} + D^* \mathbf{I}, \quad (2)$$

where  $\mathbf{I}$  is the identity matrix. In the formulation above, transverse dispersivity is assumed negligible relative to longitudinal dispersivity.

There are many adsorption equations that relate tracer fluid concentration to fracture surface concentration. The most basic form assumes equilibrium is rapid and there is a linear relationship between surface and fluid concentration. More sophisticated forms incorporate kinetics and/or non-linear isotherms (e.g., Langmuir or Freundlich). For our purposes, a non-equilibrium condition was necessary, because the half-life of the adsorption reaction was measured in the lab to be longer than the duration of the tracer experiments. From Bear (1972), a suitable non-equilibrium form for the time-derivative of surface concentration is:

$$\frac{\partial f}{\partial t} = k_{ads} (K_a c - f), \quad (3)$$

where  $k_{ads}$  and  $K_a$  are the first-order adsorption rate constant and the partition coefficient, respectively.

In order to interpret the experimental adsorbing tracer data using the above equations, the rate constant and the partition coefficient must be known independently. At the time of this writing, only preliminary laboratory measurements of these two parameters have been made. These measurements were performed in a batch reaction consisting of 100 mL fluid and a rock fragment collected from 17.4 m below ground surface at the Altona well field. The rock fragment had a nominal surface area of 26 cm<sup>2</sup>. This surface area measurement is likely much less than the reactive surface available for adsorption. However, the nominal area should be more representative of the surface area available for heat exchange, since heat diffuses rapidly through small surface heterogeneities. During the batch experiment, the fluid/rock mixture was kept at room temperature and soaked in groundwater collected from the site for 7 days prior to the addition of cesium. For the data shown in Figure 5, the partition coefficient is 14.82 cm and the rate constant is 0.62 days<sup>-1</sup>.

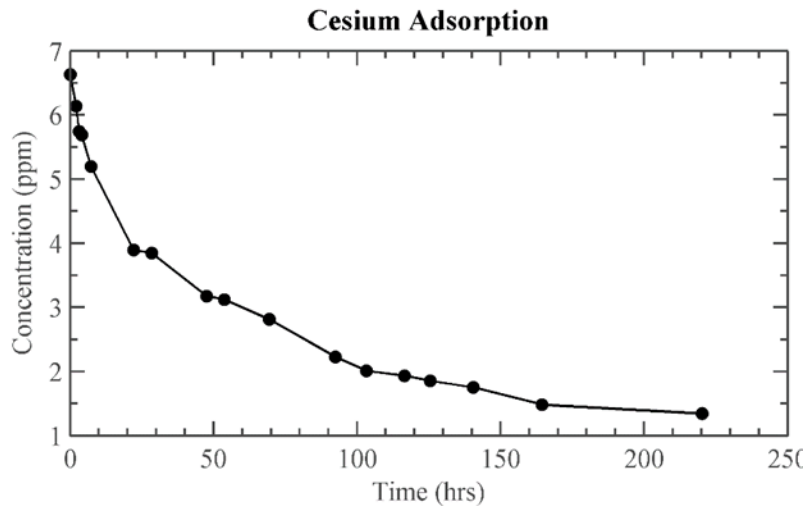


Figure 5. Lab measured adsorption of cesium onto a 26 cm<sup>2</sup> rock fragment collected from the Altona field site at a depth of 17.4 m below ground surface.

### 3.2 Field Testing

Tracer testing in the summer of 2016 was performed under forced gradient, full-dipole flow conditions at a continuous flow rate of 5.8 L/min. Produced fluids were directly reinjected into the injection well. Injection and pumping were conducted from a hydraulically isolated zone in the wellbores that were aligned with the 7.6 m deep test fracture. Hydraulic isolation in the injection and production well, and three observation wells was achieved using two modified inflatable pipe packers (Lansas Products, Lodi, California) in each well and the spacing in-between the two packers ranged from 0.2 to 0.5 m.

A salt of cesium-iodide was used as a combined inert/adsorbing tracer. Cesium, a strongly adsorbing cation, was used as the adsorbing tracer in this study due to the short residence times and the low fracture surface area anticipated. To introduce the tracer solution, a 3 L solution consisting of 217.8 mg iodide and 153.4 mg cesium was placed in a bypass PVC pipe directly inline between the injection and production well. When the tracer was ready to be injected, two valves were opened to allow flow through the bypass pipe. The bypass pipe minimized disturbance to the subsurface hydraulic gradient field that may have resulted from other means of introducing tracer, such as gravity drainage of the tracer solution through a funnel into the top of the injection well.

Groundwater samples were collected in 15 mL polypropylene conical centrifuge tubes (Corning™ Falcon™). Samples were stored on ice until the time of analysis. Cesium and Iodide were analyzed via inductively coupled plasma mass spectrometry (Element 2™ ICP-MS, Thermo Fisher Scientific Inc., MA, USA).

### 3.3 Computational Reservoir Modeling

Computational modeling of fluid, heat, and tracer transport in a discrete fracture with heterogeneous permeability was accomplished using a finite element method (FEM) solver developed by our group (Fox et al., 2015; Hawkins et al., 2017b). The model was used to simulate the effects of varying aperture distributions on the spatial distribution of heat exchange, thermal breakthrough, and tracer RTD. The heat transport model is a numerical model utilizing a hybrid finite element and boundary element method model for discretely fractured geothermal reservoirs. Two-dimensional fluid flow in the plane of the fracture is solved via the FEM while three-dimensional heat conduction in the rock matrix is captured through a boundary element treatment. The rock matrix surrounding the discrete fractures is assumed to be impermeable with respect to fluid flow.

Thermal conductivity of the Potsdam Sandstone at the Altona site was measured using the RK-1 Rock Sensor Package of the KD2 Pro manufactured by Decagon Devices. A value of 7.6 W/m-K was recorded in a rock sample collected from ground surface at the well field. The measured thermal conductivity is slightly greater than the maximum value for sandstone published in Robertson (1988) which ranges from 5 W/m-K to 7.5 W/m-K for sandstones with 60-90% quartz, 0-10% matrix porosity, and water filled pores. Density of the Potsdam Sandstone was determined to be 2.5 g/cm<sup>3</sup> by weighing a rock sample collected at ground surface and measuring its volumetric displacement in water. Specific heat was assumed to be 930 J/kg-K based on reported average values of sandstone in Robertson (1988). Specific heat and density of water was assumed to be 4200 J/kg-K and 1 g/cm<sup>3</sup>, respectively, appropriate for the temperature conditions at Altona.

### 3.4 Inverse Model

The challenge in identifying a representative fracture aperture field is that the number of unknown variables is large. For a typical computational mesh used at the Altona field site, there are approximately 9000 nodes in the computational mesh that are used to capture the spatial variability of fracture aperture. Therefore, an attempt to identify a representative aperture distribution by identifying a unique fracture aperture for each node is unrealistic considering the computational time required and the lack of influence a single node has on tracer transport.

The inversion procedure utilized in this study intends to reduce the computational time requirements by varying spatially correlated regions of the model domain using a statistical analysis commonly referred to as Principal Component Analysis (PCA). PCA reduces the complexity of a dataset by isolating correlated features that produce the most variance among the independent variables (i.e. fracture apertures). This method is explained in detail in Section 3.4.2.

#### 3.4.1 Self-Affine Rough-Walled Fractures

Naturally occurring fractures are known to have rough surfaces producing a spatially variable fracture aperture. In addition to being heterogeneous, fracture core samples have revealed that fracture apertures are also spatially correlated and self-affine (e.g., Boffa et al., 1999; Brown et al., 1986; Glover et al., 1998; Plouraboué et al., 1995; Ponson et al., 2007; Schmittbuhl et al., 1993, 1995, 2008). The spatial correlation of an aperture field is described by a spatial correlation function and a Hurst or roughness coefficient,  $\zeta$ . The variogram function,  $\gamma$ , required for describing the spatial correlation is

$$\gamma(\mathbf{r}') \equiv \left\langle [h(\mathbf{r}) - h(\mathbf{r} + \mathbf{r}')]^2 \right\rangle = 2 \left[ \langle h^2 \rangle - \langle h(\mathbf{r})h(\mathbf{r} + \mathbf{r}') \rangle \right] \quad (4)$$

where  $h$  is the local aperture fluctuation,  $\mathbf{r}'$  is the displacement from  $\mathbf{r}$ , and  $\mathbf{r}$  is a point on the surface of the fracture. The variogram function is said to have a self-affine geometry if it has a scaling behavior that follows

$$\gamma(\mathbf{r}') = C |\mathbf{r}'|^{2\zeta}. \quad (5)$$

Core samples have shown Hurst coefficients that range from 0.5 for sandstone (e.g., Boffa et al., 1999; Ponson et al., 2007) to 0.8 for granite (e.g., Schmittbuhl et al., 1993, 1995; Plouraboué et al., 1995). A surface with a lower Hurst coefficient is increasingly rough.

Hypothetical self-affine fracture aperture distributions were generated using an algorithm modified from Méheust and Schmittbuhl (2001). The distribution is constructed by random seeding using Fast Fourier Transforms (FFT) to obtain isotropic self-affine fracture aperture fields on rectangular fractures. The mesh utilized in this study was circular, so the rectangular fractures were modified by only incorporating the areas inscribed by a circle of length  $2R$ , where  $R$  is the circle radius.

### 3.4.2 Principal Component Analysis

Principal Component Analysis (PCA) is a statistical tool commonly used in engineering sciences to identify the dominant behavior of a dataset consisting of two or more independent variables. PCA is performed by first determining the covariance matrix of the data set. Then, the eigenvectors and eigenvalues of the covariance matrix are calculated. Each eigenvector represents a “mode” of the dataset and the matrix is organized from the most to least dominant mode based on the magnitude of the eigenvalues. For spatially correlated fractures, the mode with the largest eigenvalue corresponds to spatial variations over relatively large areas of the fracture. The benefit of PCA for the purpose of identifying representative aperture distributions is that it permits parameter reduction and allows an inversion method to vary large spatially correlated regions of the aperture at once.

For a data set  $X_{ij}$  comprised of  $n$  independent variables where each variable has a mean of zero across  $m$  observations, the covariance matrix,  $C_{ij}$ , between variable  $i$  and  $j$  is

$$C_{ij} = \sum_{k=1}^m X_{ik}X_{jk}. \quad (6)$$

For a discrete heterogeneous fracture represented by nodes on a computational mesh,  $n$  is the number of nodes and  $m$  is the number of aperture fields generated. Once the eigenvectors (or “modes”) and eigenvalues (or “coefficients”) of the covariance matrix have been determined, an aperture field in the matrix of observations can be reproduced by knowing the modes of the entire dataset and the coefficients for the specific aperture field:

$$w_i = \sum_{j=1}^p \Phi_{ij}\alpha_j + \langle w \rangle, \quad (7)$$

where  $w_i$  is the fracture aperture at node  $i$ ,  $\Phi_{ij}$  is the matrix of PCA modes,  $\alpha_j$  are the coefficients of the PCA modes, and  $\langle w \rangle$  is the mean fracture aperture. If  $p$  is equal to  $n$ , the total number of nodes, then the original dataset is replicated identically. If, however, a reduced order model is desired,  $p$  can be selected for any integer value greater than zero and less than  $n$ . The lower the value of  $p$ , the more the fracture aperture distribution is simplified by neglecting small spatial variations. In addition, entirely new aperture distributions can be produced by altering the magnitude of the mode coefficients. Any new distribution will have a unique aperture field, but the eigenvectors of its covariance matrix (i.e. its PCA modes) are identical to the original data set.

### 3.4.3 Genetic Algorithm

There are several challenging aspects of successfully employing an inverse method for determining aperture fields, including: (1) it is non-linear; (2) there are a large number of unknown variables; (3) the fracture aperture field is non-unique; and (4) there are likely many local minimums of the objective function. For these reasons, a Genetic Algorithm (GA) was selected as the ideal inverse search method. A GA is a metaheuristic stochastic global optimizer that mimics natural selection to minimize an objective function  $f(x_j)$  where  $x_j$  is a set of parameter values. The GA is similar to natural selection in that you select an initial population and generate a new generation by breeding and mutation. New generations are created until the objective function has been reduced below a designated threshold or the number of specified generations has been reached.

For this study, the parameter values for the GA are the PCA mode coefficients and the objective function is the sum of square errors between the measured and simulated tracer RTDs for both the inert and adsorbing tracer. Each new generation was produced by combining mode coefficients of the two optimal individuals. For each GA parameter of a new individual, the mode coefficient has a fifty percent chance of being the corresponding coefficient of one of the two parents. This procedure is followed until the desired number of populations in the new generation has been reached. A mutation is performed only if a specified number of generations have been produced without a reduction in the objective function. In this study, a mutation was performed by multiplying each variable in a population by a random number between 0.9 and 1.1.

## 4. RESULTS

### 4.1 Tracer Tests

Results of the tracer test are shown in Figure 6. Breakthrough curves are plotted as  $c/m_0$ , where  $c$  is the measured effluent tracer concentration and  $m_0$  is the tracer mass injected. Tracer test conditions are summarized in Table 1. Well 204 and Well 304, shown in

Figure 1 and Figure 3, are the injection and production well, respectively. The average extraction/injection rate was 5.8 L/min and the well separation was 14 m. To determine the mass recovered and mean residence time, a deconvolution of the reinjected tracer was performed following Shook and Forsmann (2005). After deconvolution, the mean tracer residence time was found to be 38 mins and the mass recovered for iodide and cesium are 64 and 24%, respectively.

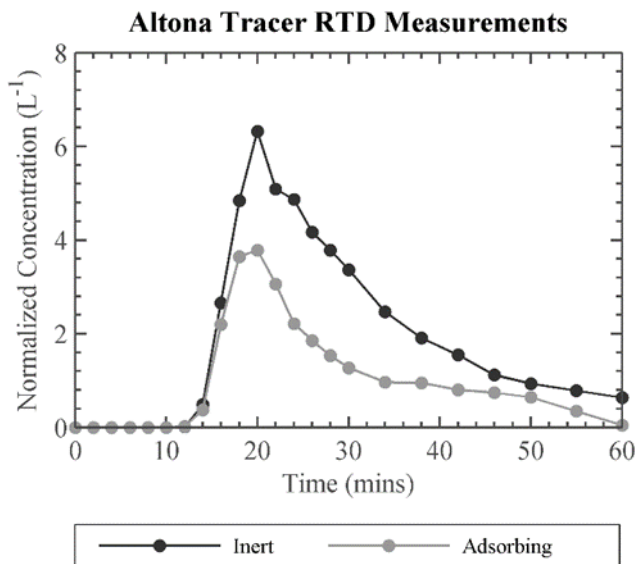


**Figure 6. Measured tracer Residence Time Distribution (RTD) at the Altona field site. Iodide and cesium were used as the inert and adsorbing tracer, respectively. The points plotted reflect modifications to the measured data to remove the effect of tracer reinjection on the RTD following the approach described in Shook and Forsmann (2005). Tracer concentration is normalized by dividing the measured concentration by the mass of tracer injected with units of L<sup>-1</sup>.**

**Table 1. Tracer test conditions and results**

Volumetric Flow Rate =	5.8	L/min
Mass Injected (I) =	217.8	mg
Mass Injected (Cs) =	153.4	mg
Mean Residence Time =	38	mins
Mass Recovered (I) =	64%	
Mass Recovered (Cs) =	24%	

#### 4.2 Fracture Aperture Field

The inverse model was used to identify a representative fracture aperture field based on matching simulated to measured inert and adsorbing tracer data. The inverted variables included the mean fracture aperture, longitudinal dispersivity, and the coefficients of 1000 modes of the PCA. Selecting an appropriate number of modes to include in the inverse model is somewhat arbitrary. Sensitivity analysis showed that modes beyond the 100<sup>th</sup> greatest eigenvalue did not have a strong influence on the objective function of the GA. The computational efficiency of the GA is weakly influenced by the number of modes, so a conservative number of 1000 modes was selected in this study. The roughness coefficient for the self-affine fracture was allowed to deviate from the sandstone Hurst roughness coefficient reported in literature, which is typically 0.5.

A representative fracture aperture field was identified by fitting simulated to measured inert and adsorbing tracer RTD. Using a population of 20 individuals and 100 generations, the GA produced a sufficient fit to the measured tracer data (Figure 7). The fracture aperture field produced reveals a linearly extensive, narrow channel (~1-2 m) directly between the injection and production well (Figure 8). The flow channel fracture aperture is roughly 6 to 7 mm while the low aperture region surrounding it is roughly 0.2 to 1 mm. The inverse model resulted in a mean fracture aperture of 3.3 mm and longitudinal dispersivity of 0.13 m.

The initial Hurst roughness coefficient selected was 0.5. However, this value did not produce a sufficiently low FWA to fit the measured adsorbing tracer data. It was found that a rougher aperture distribution was necessary to fit the data with a Hurst coefficient of 0.15.

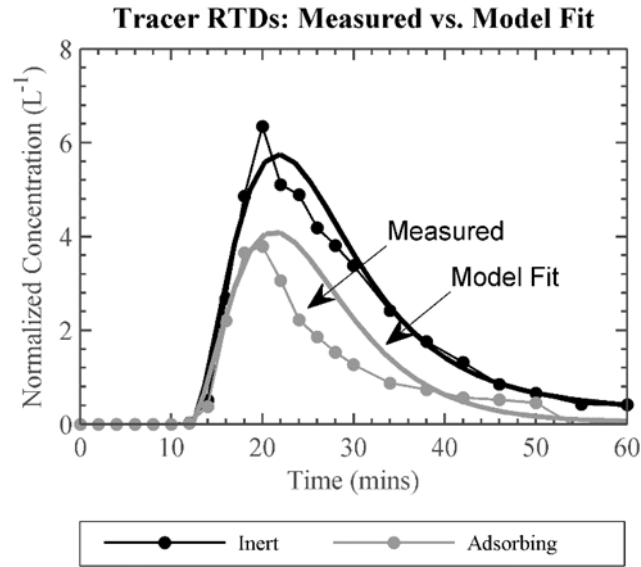


Figure 7. Measured vs. model fit for the inert tracer iodide and the adsorbing tracer cesium. The model fit used the sum of square errors of the inert and adsorbing tracer RTDs

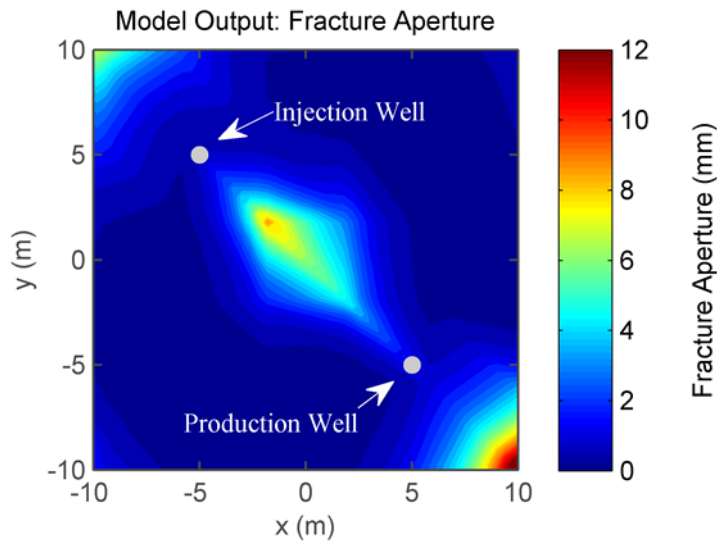
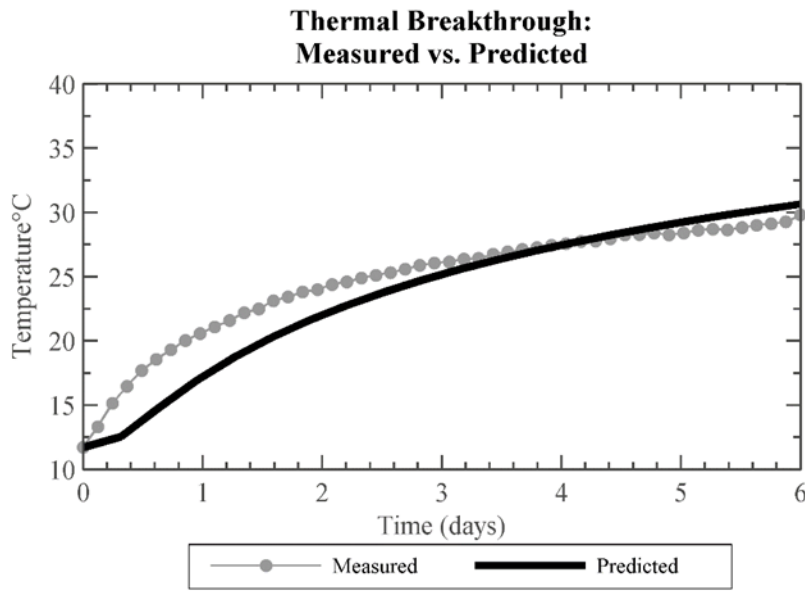


Figure 8. Inverse model output of a representative two-dimensional fracture aperture field using the inert tracer iodide and the adsorbing tracer cesium.

#### 4.3 Thermal Performance

The fracture aperture distribution identified via the inverse model (Figure 8) revealed a large, narrow flow channel directly between the injection well and production well. This aperture field was subsequently used in the heat transport model to forecast thermal breakthrough at the production well and predict the spatial distribution of temperature rise within the plane of the fracture. Predicted thermal breakthrough occurs within 3 hr of circulating hot water (Figure 8). By the end of the experiment (6 days), predicted production well temperature reaches 30.7 °C. In the plane of the fracture, the spatial distribution of heat exchange followed the narrow path of the flow channel (Figure 10).



**Figure 9. Predicted vs. measured thermal breakthrough at the production well during 6 days of continuous hot water injection. Thermal breakthrough was predicted based on a heat transport model using the aperture distribution shown in Figure 8, which was the output of the inverse model fit shown in Figure 7.**

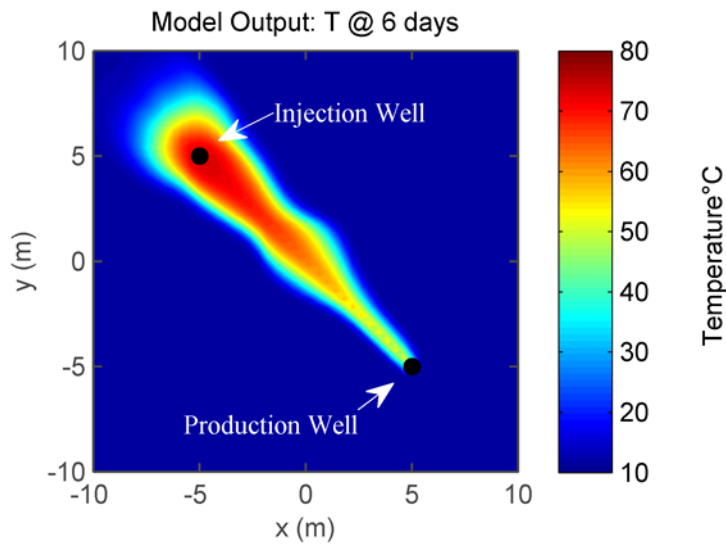


**Figure 10. Predicted temperature spatial distribution in the two-dimensional plane of the fracture after 6 days of continuous hot water injection. The prediction is based on the fracture aperture distribution shown in Figure 8 which resulted from the inverse model output shown in Figure 7.**

The measured onset of thermal breakthrough occurred after 44 mins of hot water injection (Figure 9). The initial rate of temperature rise is rapid and flattens substantially after roughly 1 day of heating. At the end of the experiment (6 days), measured temperature at the production well is 29.8 °C.

**5. DISCUSSION**

The results of the inverse model reveal that circulation between the injection well and production well at the Altona field site is prone to flow channelization and, as a consequence, premature thermal breakthrough would be likely if this geothermal analog were a commercial operation. The aperture field produced from the inverse model shows a narrow (roughly 1-2 m) region of large (roughly 6 to 7 mm) fracture aperture directly connecting the injection well and production well (Figure 8). A prediction of the spatial distribution of temperature rise in the plane of the fracture based on this aperture distribution demonstrates that heat exchange is limited to the width of the flow channel (Figure 10).

Forecasted thermal breakthrough generally agrees with measured temperature rise recorded in the production well during continuous hot water injection at the Altona field site (Figure 9). Both predicted and measured thermal breakthrough occur within roughly 3 hr of initiating hot water injection. Predicted thermal breakthrough agrees with measured better after roughly 2.5 days. By the end of the experiment, the inverse model predicts temperature in the production well is 30.7 °C which is nearly identical to the measured temperature (29.8 °C).

The spatial distribution of fluid flow revealed by the heat transport model agrees generally with both Ground Penetrating Radar (GPR) imaging of saline tracer flow paths (Figure 2) and the spatial distribution of heat exchange recorded via Fiber-Optic Distributed Temperature Sensing (FODTS) (Figure 3). The GPR imaging and the heat transport simulation both suggest that flow was concentrated through a narrow (1-2 m) channel directly between the two wells. In addition, the FODTS data also show that heat transport was limited to the same narrow flow channel.

The fracture aperture identified via the inverse model (Figure 8) was substantially rougher ( $\zeta=0.15$ ) than measured roughness reported in literature for sandstone ( $\zeta=0.5$ ). The GPR background imaging of fracture aperture (Figure 2), however, was consistent with literature values ( $\zeta=0.45$ ). The conflicting values for roughness may suggest that flow channeling at Altona did not result from fracture aperture variations. An alternative explanation may be that vertical fracture joints intersecting the target fracture acted as barriers to flow across them. Evidence supporting this explanation are reported in Talley (2005) where numerous vertical joints oriented in an E-W direction were identified at ground surface. The distance between vertical joint expressions range from 0.1 to 2.6 m with a mean of 1.0 m. These distances are relatively similar to the width of the flow channel identified via FODTS, GPR, and computational simulations (~1-2 m).

## 6. CONCLUSION

An inverse model for identifying spatially varying permeability fields successfully forecasted the occurrence of premature thermal breakthrough in a geothermal analog field site. The inversion was performed based on minimizing the sum of square errors between simulated and measured tracer RTDs using both inert and adsorbing tracers. Principal Component Analysis (PCA) was used to focus the inverse model on varying spatially correlated regions of the permeability field. A Genetic Algorithm (GA) optimizer was used to inversely solve for the coefficients of the PCA modes as well as the mean fracture aperture and longitudinal dispersivity. The reaction rate and equilibrium partition coefficient used in the reactive adsorption model were measured in a laboratory batch reactor experiment.

Two-dimensional simulations of heat transport based on the fracture aperture field produced from the inverse model agreed well with Ground Penetrating Radar (GPR) imaging of saline tracer flow paths. Despite the opposing direction of fluid flow in the two experiments, both data sets show that a narrow flow channel less than 2 m in width was responsible for the occurrence of rapid thermal breakthrough measured at the Altona field site. In addition, Fiber-Optic Distributed Temperature Sensing (FODTS) was used to measure the spatial distribution of heat exchange between flowing fluids and the bulk rock matrix. These data are consistent with GPR data and the inverse model output revealing that heat transfer was greatest in a narrow, direct path between injection and production well.

The narrow channel that dominates the spatial distribution of fluid flow at Altona may not have been caused by a spatially varying fracture aperture field. Despite good agreement between fracture roughness measured via GPR ( $\zeta=0.45$ ) and literature values for sandstone ( $\zeta=0.5$ ), the inverse model required a much rougher fracture ( $\zeta=0.15$ ) to fit the measured inert/adsorbing tracer RTDs. Future research will investigate whether or not the vertical fracture joints expressed at ground surface could be influencing the spatial distribution of fluid flow at Altona. Previous investigations of the vertical fractures at Altona found that the mean and maximum distance between these fractures measured at ground surface are 1 to 2.6 m, respectively. That range is consistent with the results of this study, which show that the flow channel is roughly 1 to 2 m.

The results of this study suggest that thermal breakthrough can be predicted, *a-priori*, using an inverse model for spatially varying permeability fields combined with inert and adsorbing tracers. This was demonstrated at the Altona field site, which is a meso-scale geothermal analog. To the best of the authors' knowledge, this is the first successful field application of adsorbing tracers as a means of forecasting heat transfer between fluids in fractured rock and the bulk rock matrix. In addition, the aperture field identified via the inverse model successfully predicted the occurrence of premature thermal breakthrough. While these results are encouraging, commercial geothermal reservoirs operate on much larger spatial and temporal scales with, ideally, more than a single fracture. Subsequent research articles will report on our continued investigation into reactive tracers and inverse models used in conditions more consistent with commercial geothermal reservoirs.

## ACKNOWLEDGEMENTS

This material is based upon work supported by the U.S. Department of Energy, Office of Energy Efficiency and Renewable Energy (EERE), Office of Technology Development, Geothermal Technologies Program, under Award Numbers DE EE0006764 and DE EE0002767. Additional financial assistance was provided by the National Science Foundation's Earth Energy IGERT program and the Cornell Energy Institute. The authors thank the William H. Miner Agricultural Research Institute for providing access to their facilities, including their Environmental Laboratory and the Altona Flat Rock site. The authors would also like to thank Ivan Beentjes, Sean Hillson, Koenraad Beckers, and Maciej Lukawski for providing much appreciated assistance during field experiments.

## REFERENCES

Axelsson, G., Flovenz, O.G., Hauksdottir, S., Hjartarson, A., and Liu, J.: Analysis of Tracer Test Data, and Injection-Induced Cooling, in the Laugaland Geothermal Field, N-Iceland, *Geothermics*, **30**, (2001), 573-589.

- Axelsson, G., Björnsson, G., and Montalvo, F.: Quantitative Interpretation of Tracer Test Data, *Proceedings*, World Geothermal Congress, Antalya, Turkey (2005).
- Becker, M. W., and Tsoflias, G.P.: Comparing Flux-Averaged and Resident Concentration in a Fractured Bedrock using Ground Penetrating Radar, *Water Resources Research*, **46**, (2010).
- Becker, M.W., Remmen, K., Reimus, P.W., and Tsoflias, G.P.: Investigating Well Connectivity using Ionic Tracers, *Proceedings*, 38th Workshop on Geothermal Reservoir Engineering, Stanford University, Stanford, CA (2013).
- Bodin, J., Delay, F., de Marsily, G.: Solute Transport in a Single Fracture with Negligible Matrix Permeability: 1. Fundamental Mechanism, *Hydrogeology Journal*, **11**, (2003), 418-433.
- Boffa, J.M., Allain, C., Chertcoff, R., Hulin, J., Plouraboué, F., and Roux, S.: Roughness of Sandstone Fracture Surfaces: Profilometry and Shadow Length Investigations, *European Physical Journal B*, **7**, (1999), 179-182.
- Brown, S.R., Kranz, R., and Bonner, B.: Correlation between the Surfaces of Natural Rock Joints, *Geophysical Research Letters*, **13**, (1986), 1430-1433.
- Dagan, G.: Statistical Theory of Groundwater Flow and Transport: Pore to Laboratory, Laboratory to Formation, and Formation to Regional Scale, *Water Resources Research*, **22**, (1986), 120S-134S.
- Dean, C., Reimus, P., and Newell, D.: Evaluation of a Cation Exchanging Tracer to Interrogate Fracture Surface Area in EGS Systems, *Proceedings*, 37th Workshop on Geothermal Reservoir Engineering, Stanford University, Stanford, CA (2012).
- Fox, C.E., and Horne, R.N.: Determination of Fracture Aperture: A Multi-Tracer Approach, *Transactions – Geothermal Resources Council*, **12**, (1988), 449-456.
- Fox, D.B., Koch, D., and Tester, J.W.: The Effect of Spatial Aperture Variations on the Thermal Performance of Discretely Fractured Geothermal Reservoirs, *Geothermal Energy*, **3**, (2015), 1-29.
- Glover, P.W.J., Matsuki, K., Hikima, R., and Hayashi, K.: Fluid Flow in Synthetic Rough Fractures and Application to the Hachimantai Geothermal Hot Dry Rock Test Site, *Journal of Geophysical Research*, **103**, (1998), 9621-9635.
- Hawkins, A.J., Becker, M.W., and Tsoflias, G.P.: Evaluation of Inert Tracers in a Bedrock Fracture using Ground Penetrating Radar and Thermal Sensors, *Geothermics*, (2017a), Accepted Author Manuscript.
- Hawkins, A.J., Fox, D.B., Becker, M.W., Tester, J.W.: Measurement and Simulation of Heat Exchange in Fractured Bedrock using Inert and Thermally Degrading Tracers, *Water Resources Research*, (2017b), Accepted Author Manuscript.
- Kristjánsson, B.R., Axelsson, G., Gunnarsson, G., Gunnarsson, I., Óskarsson, F.: Comprehensive Tracer Testing in the Hellisheidi Geothermal Field in SW-Iceland, *Proceedings*, 41st Workshop on Geothermal Reservoir Engineering, Stanford University, Stanford, CA (2016).
- Méheust, Y., and Schmittbuhl, J.: Geometrical Heterogeneities and Permeability Anisotropy of Rough Fractures, *Journal of Geophysical Research: Solid Earth*, **106**, (2001), 2089-2102.
- Moench, A.F.: Convergent Radial Dispersion: A Laplace Transform Solution for Aquifer Tracer Testing, *Water Resources Research*, **25**, (1989), 439-447.
- Moench, A.F.: Convergent Radial Dispersion in a Double-Porosity Aquifer with Fracture Skin: Analytical Solution and Application to a Field Experiment in Fractured Chalk, *Water Resources Research*, **31**, (1995), 1823-1835.
- National Research Council: Rock Fractures and Fluid Flow: Contemporary Understanding and Applications, *National Academy Press*, Washington, D.C. (1996).
- Neretnieks, I.: A Note on Fracture Flow Dispersion Mechanisms in the Ground, *Water Resources Research*, **19**, (1983), 364-370.
- Olcott, P.G.: Ground Water Atlas of the United States, Reston, Virginia, (1995).
- Plouraboué, F., Kurowski, P., Hulin, J.P., Roux S., and Schmittbuhl, J.: Aperture of Rough Cracks, *Physical Review*, **51**, (1995), 1675.
- Ponson, L., Auradou, H., Pessel, M., Lazarus, V., and Hulin, J.P.: Failure Mechanisms and Surface Roughness Statistics of Fractured Fontainebleau Sandstone, *Physical Review E*, **76**, (2007).
- Rayburn, J. A., Knuepfer, P. L. K., and Franz, D. A.: A Series of Large, Late Wisconsinan Meltwater Floods through the Champlain and Hudson Valleys, New York State, USA, *Quaternary Science Reviews*, **24**, (2005), 2410-2419.
- Reimus, P., Pohll, G., Mihevc, T., Chapman, J., Haga, M., Lyles, B., Kosinski, S., Niswonger, R., and Sanders, P.: Testing and Parameterizing a Conceptual Model for Solute Transport in a Fractured Granite using Multiple Tracers in a Forced-Gradient Test, *Water Resources Research*, **39**, (2003), 1356.
- Robertson, E.C.: Thermal properties of rocks. Report U.S. Department of the Interior, Report 88-441, Geological Survey, Reston, VA (1988)
- Robinson, B.A., Tester, J.W., and Brown, L.F.: Reservoir Sizing using Inert and Chemically Reacting Tracers, *SPE Formation Evaluation*, **3**, (1998), 227-234.

- Schmittbuhl, J., Gentier, S., and Roux, S.: Field Measurements of the Roughness of Fault Surfaces, *Geophysical Research Letters*, **20**, (1993), 639-641.
- Schmittbuhl, J., Schmitt, F., Scholz, C.: Scaling Invariance of Crack Surfaces, *Journal of Geophysical Research: Earth Surface*, **100**, (1995), 5953-5973.
- Schmittbuhl, J., Steyer, A., Jouniaux, L., and Toussaint, R.: Fracture Morphology and Viscous Transport, *International Journal of Rock Mechanics and Mining Sciences*, **45**, (2008), 422-430.
- Shook, G.M.: Predicting Thermal Breakthrough in Heterogeneous Media from Tracer Tests, *Geothermics*, **30**, (2001), 573-589.
- Shook, G.M.: A Simple, Fast Method of Estimating Fractured Reservoir Geometry from Tracer Tests, *Transactions - Geothermal Resources Council*, **27**, (2003).
- Shook, G.M., and Forsmann, J.H.: Tracer Interpretation using Temporal Moments on a Spreadsheet, *Technical Report*, U.S. Department of Energy – Geothermal Technologies Program, Idaho National Laboratory, (2005).
- Talley, J.: Imaging channelized flow in fractured rock using surface GPR, *M.S. Thesis*, State University of New York, Buffalo, (2005).
- Talley, J., Baker, G., Becker, M.W., and Beyrle, N.: Four Dimensional Mapping of Tracer Channelization in Subhorizontal Bedrock Fractures using Surface Ground Penetrating Radar, *Geophysical Research Letters*, **32**, (2005).
- Tester, J.W., Robinson, B., and Ferguson, J.H.: Inert and Reacting Tracers for Reservoir Sizing in Fractured, Hot Dry Rock Systems, *Proceedings*, 11th Workshop on Geothermal Reservoir Engineering, Stanford University, Stanford, CA (1986).
- Tsang, C.F., and Neretnieks, I.: Flow Channeling in Heterogeneous Fractured Rocks, *Reviews of Geophysics*, **36**, (1998), 275-298.
- Tsoflias, G.P., and Becker, M.W.: Ground-Penetrating Radar Response to Fracture-Fluid Salinity: Why Lower Frequencies are Favorable for Resolving Salinity Changes, *Geophysics*, **73**, (2008), J25-J30.
- Tsoflias, G.P., Baker, M., and Becker, M.W.: Imaging Fracture Anisotropic Flow Channeling using GPR Signal Amplitude and Phase, *Proceedings*, SEG Technical Program Expanded Abstracts, Houston, TX (2013).
- Tsoflias, G.P., Perll, C., Baker, M., and Becker, M.W.: Cross-Polarized GPR Imaging of Fracture Flow Channeling, *Journal of Earth Science*, **26**, (2015), 776-784.
- Vetter, O.J., and Crichlow, H.B.: Injection, Injectivity and Injectability in Geothermal Operations: Problems and Possible Solutions (Phase I – Definition of the Problems, *Technical Report*, U.S. Department of Energy – Geothermal Energy, SAN-2044-1, (1979).
- Williams, M.D., Vermeul, V.R., Reimus, R.W., Newell, D., and Watson, T.B.: Development of Models to Simulate Tracer Behavior in Enhanced Geothermal Systems, PNNL-19523; OSTI ID: 992377.
- Wooding, R.A.: Instability of a Viscous Fluid of Variable Density in a Vertical Hele-Shaw Cell, *Journal of Fluid Mechanics*, **7**, (1960), 501-515.